Fuel 135 (2014) 359–373

Contents lists available at ScienceDirect

Fuel

journal homepage: www.elsevier.com/locate/fuel

Nano-scale texture and porosity of organic matter and clay minerals in organic-rich mudrocks

Utpalendu Kuila [a,1], Douglas K. McCarty [b,*], Arkadiusz Derkowski [a], Timothy B. Fischer [b], Tomasz Topór [a], Manika Prasad [c]

[a] Institute of Geological Sciences, Polish Academy of Sciences, Senacka 1, 31-002 Krakow, Poland
[b] Chevron Energy Technology Company (ETC), Houston, TX, United States
[c] Colorado School of Mines, Golden, CO, United States

HIGHLIGHTS

- Clay hosted porosity is the fundamental textural control of mudrock nanostructure.
- Clay porosity in immature mudrocks may be open or partially filled by organics.
- Organic matter in the immature mudrocks does not have any open nano-scale porosity.
- Organic matter in mature mudrocks have significant pore volume with diameter <5 nm.
- High-pressure methane adsorption is controlled by organic matter porosity.

GRAPHICAL ABSTRACT

Pore size distribution of samples showing significant pore volume decrease below 5 nm pore size upon organic matter removal by NaOCl treatment. Blue circles represents the natural aliquot while the red triangles are the organic removed aliquot. I+S = illite + smectite clay group in wt.%; TOC = Total Organic Carbon in wt.%; Eff. = organic matter removal efficiency in %; HI = Hydrogen Index in mg HC/g TOC.

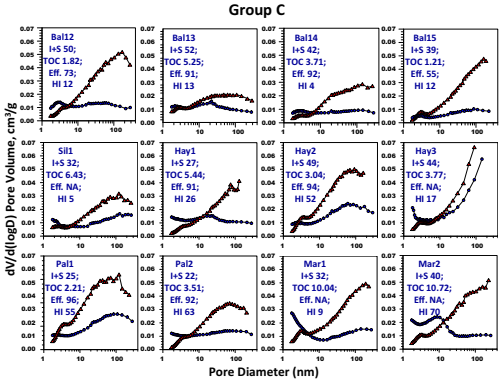

ARTICLE INFO

Article history:
Received 17 April 2014
Received in revised form 10 June 2014
Accepted 12 June 2014
Available online 8 July 2014

Keywords:
Organic-rich mudrocks
Pore-size distribution

ABSTRACT

Speculation exists in the oil and gas shale community about the form and distribution of the organic matter within the nanometer scale texture of mudrocks. In addition, the presence of micropore and mesopore networks either exclusively within the organic matter or as pore systems in the mineral components of these formations are not well understood. There is little published quantitative data with respect to the development of porosity in organic matter (OM) with thermal maturity in a burial diagenetic sequence. This paper presents a comparative study of pore-size distribution (PSD) in a burial sequence from the Baltic Basin, along with a selection of samples from other unconventional hydrocarbon reservoirs of various age and origin. Methods include quantitative mineral analysis by X-ray diffraction (XRD), RockEval

Abbreviations: TOC, total organic carbon; OM, organic matter; FESEM, field emission scanning electron microscopy; SGA, subcritical gas adsorption; XRD, X-ray diffraction; HI, Hydrogen Index; I–S, mixed-layered illite–smectite; I+S, total illite + smectite group of clays; SSA, specific surface area; PSD, pore-size distribution; BET, Brunauer–Emmett–Teller (BET) theory; BJH, the Barret, Joyner, and Halenda technique to obtain pore-size distribution; P/P_0, relative pressure in the SGA measurement, P is the absolute equilibrium pressure and P_0 is the saturation pressure of N_2 at 77 K; $Vp_{<5nm}$, total pore volume of pores with diameter less than 5 nm.

* Corresponding author. Tel.: +1 7139546298.
E-mail address: dmccarty@chevron.com (D.K. McCarty).
[1] Formerly with Colorado School of Mines.

http://dx.doi.org/10.1016/j.fuel.2014.06.036
0016-2361/

Subcritical nitrogen gas adsorption
Clay minerals
Organic matter

pyrolysis, and subcritical gas-adsorption (SGA) analysis with N_2 at 77.3 K. SGA with N_2 is effective in quantifying the volume of small pores that are below the detection limit of imaging techniques. Analyses were performed on aliquot samples in the natural state and after OM removal by treatment with buffered sodium hypochlorite (NaOCl).

The results indicate that the clay hosted micro- and mesoporous network forms the textural structure of mudrocks at the nanometer scale. The distribution of OM with respect to the clay microstructure is heterogeneous. OM exists as separate particles or laminations where clay porosity may be open to adsorption, or OM can partially or completely occupy the space between clay aggregates within dimensions <5 nm. The presence of micropores and fine mesopores within the OM itself are only observed in thermally mature samples where the RockEval Hydrogen Index (HI) is <100. The relative abundance of micro- and fine mesopores in the thermally mature mudrocks is controlled by both the clay and the OM content. Comparison of high-pressure methane adsorption measurements from OM-removed and natural aliquots demonstrate that thermally mature OM with well-developed microporosity has significantly greater adsorbing potential than clay-hosted porosity with comparable volume.

1. Introduction

One of the important characterization parameters in evaluating self-sourcing reservoirs such as gas shale plays is the total organic carbon (TOC), which is an indicator of the amount of organic matter (OM) present in these mudrock reservoirs. The amount of OM present is directly correlated with several rock properties, including total porosity [1,2], microporosity [3,4], total gas content [5], methane sorption capacity [3,4,6–8], and the bulk rock elastic properties [9–11]. Therefore, a thorough understanding of the properties of OM is critical to predicting the physical properties of the whole rock. There is no agreement as to how these OM properties change during the thermal evolution in sedimentary basins, especially the pore structure. Recent studies using advanced imaging techniques have reported the presence of nanometer scale pore networks in the OM that are present in thermally mature mudrocks [1,2,12–14]. However, the detection limit of the most advanced imaging instruments, like field emission scanning electron microscopy (FESEM), is about 4–7 nm and undetectable pores can comprise up to 95% of the total porosity [2]. The detectable pores in these studies are only limited to visual density contrasts within the OM at ambient laboratory conditions. Subcritical gas adsorption (SGA) techniques using nitrogen gas at 77 K provides an alternative which can investigate the distribution of fine pores, which are undetectable by imaging studies as well as quantifying the whole rock volume of the micropore interval.

Previous SGA-N_2 studies on both thermally immature oil shale and modern ocean bottom sediments did not reveal any evidence of primary open pores within the immature OM [15–19]. Laboratory pyrolysis experiments on immature OM rich oil shale samples indicated that the development of an open pore structure only occurs at elevated temperatures above ~400 °C [11,16,20–22]. These studies suggest that the reported OM porosity in thermally mature mudrocks developed at some stage of diagenesis. Some studies suggest OM porosity develops at the beginning of the gas window [13,23], while others suggest it is at the beginning of the oil window [14,24,25]. There is no clear correlation reported between the abundance and morphology of OM porosity with increasing thermal maturity [2,13].

In addition to that in the OM-hosted pore system, there is a significant volume of nano and microscale pore-structure within clay mineral aggregates in mudrocks [26]. The relative contribution of OM-hosted porosity as compared to clay-hosted porosity to bulk mudrock porosity is also debated [12,13]. Curtis et al. [13] reported that OM porosity is dominant in Barnett, Kimmeridgian, Woodford, and Horn River shales, whereas porosity in the Haynesville Shale is dominated by the clay nanostructure. Milliken et al. [2] reported that OM porosity visible in FESEM accounts for 2–32% of the total helium porosity measured for a set of samples from the Marcellus Shale, but that the majority of OM hosted porosity was not detected. There are few studies that quantitatively differentiate between the respective contributions of OM hosted and clay aggregate porosity to the total pore volume of rock.

Understanding the relative contribution of OM hosted pores to the total pore volume, particularly in the micropores and fine mesopore range, have critical significance in estimating the storage and production properties of these unconventional reservoirs. A large fraction of the gas is stored as 'sorbed' gas, which is adsorbed to the large specific surface areas associated with the micropores and fine mesopores. The methane adsorption capacity of the mudrocks shows a strong positive correlation with the TOC [3,6–8]. However, clay minerals may also provide additional sorption capacities [4,6,27–29] due to their fine-scale pore structure and associated high external surface areas. The sorption energies or the isosteric heats of adsorption for methane on OM is almost double that than with clay minerals [7,29]. Due to the difference in surface energy, differentiating and quantifying the pore volume in OM and that within clay aggregates and other inorganic components is critical for modeling gas adsorption and desorption processes in mudrocks, which has significant production implications.

The objective of this study is to obtain quantitative pore structure parameters, including the specific surface area and pore-size distribution (PSD) between the OM and inorganic components of rocks with contrasting thermal maturity and bulk composition. In this study, pore structure is compared from aliquot samples before and after removing the OM from the natural sample. By comparing the pore structure attributes before and after OM removal the amount of porosity contained in the OM can be quantified, thereby allowing for correlation of OM porosity and thermal maturity as determined by other analytical methods such as RockEval pyrolysis.

2. Methods and materials

2.1. Samples

Twenty-three mudrock samples (chips from whole core) for this study came from five different shale-play basins from North America and Europe (Table 1). The sample labels indicate abbreviated form of the geologic location or formation, e.g., Sil, Hay, Pal, Mar and Bal stands for Silurian Shale from Eastern Europe, Haynesville Shale, Paleozoic Shale from North America, Marcellus Shale and Baltic Basin shales, respectively. The samples were characterized for quantitative mineral composition by X-ray diffraction (XRD)

Table 1
Mineralogy from quantitative phase analysis using X-Ray diffraction (QXRD) techniques, TOC content and RockEval parameters of the investigated samples. Well names and core depths for Baltic Basin samples are mentioned. Qtz = Quartz; Carb = Total Carbonate; I+S = total illite + smectite group of clays; TOC = Total Organic Carbon; HI = Hydrogen Index; OI = Oxygen Index; NA = Not Available.

Sample name	Sample description	Qtz + Feldspar (wt.%)	Carb (wt.%)	Pyrite (wt.%)	I+S (wt.%)	Total Clay (wt.%)	TOC-Natural aliquot (wt.%)	S1 (mg HC/g rock)	S2 (mg HC/g rock)	S3 (mg CO_2/g rock)	Tmax (°C)	HI (mg HC/g TOC)	OI (mg CO_2/g TOC)	TOC (NaOCl-treated aliquot (wt.%))	OM removal efficiency (%)
Sil1	Eastern European Silurian Shale	52	2	1.9	32	36	6.43	0.06	0.3	0.29	–	5	5	NA	NA
Hay1	Haynesville	20	35	3.8	27	32	5.54	2.32	1.43	0.54	334	26	10	0.48	91
Hay2	Haynesville	35	12	2.0	49	51	3.04	1.47	1.57	0.39	343	52	13	0.18	94
Hay3	Haynesville	34	14	2.0	45	50	3.77	0.1	0.65	0.15	522	17	4	NA	NA
Pal1	North American Palaeozoic Shale	24	39	5.0	26	32	2.21	1.31	1.22	0.28	457	55	13	0.09	96
Pal2	North American Palaeozoic Shale	43	28	4.0	23	26	3.51	1.59	2.2	0.39	483	63	11	0.29	92
Mar1	Marcellus	39	8	16.0	29	37	10.04	0.33	0.95	0.31	309	9	5	NA	NA
Mar2	Marcellus	36	6	12.0	41	46	10.72	6.01	7.51	0.27	470	70	3	NA	NA
Bal1	Baltic Basin: Gołdap IG-1, 1415 m	41	5	0.8	43	54	5.65	0.6	25.85	2.48	423	458	44	1.53	73
Bal2	Baltic Basin: Gołdap IG-1, 1416 m	41	6	7.0	38	43	5.26	0.39	18.98	2.62	421	361	50	0.71	86
Bal3	Baltic Basin: Barciany 1, 1591 m	36	8	1.0	46	55	2.20	0.16	8.82	1.28	435	401	58	0.73	67
Bal4	Baltic Basin: Bartoszyce IG-1, 1795.6 m	37	1	1.0	48	59	5.21	0.5	20.94	1.73	431	402	33	1.49	71
Bal5	Baltic Basin: Sępopol 2, 1804.5 m	37	7	0.8	37	55	1.51	0.11	4.85	0.98	436	322	65	0.91	40
Bal6	Baltic Basin: Olsztyn IG-2, 2356.2 m	35	5	3.0	35	57	1.93	0.12	3.76	0.53	442	195	27	0.72	63
Bal7	Baltic Basin: Białogóra 1, 2613 m	30	1	2.0	57	66	6.12	0.87	12.42	0.39	451	203	6	2.58	58
Bal8	Baltic Basin: Białogóra 1, 2623 m	24	39	1.0	30	37	0.39	0.09	0.56	0.32	438	145	83	0.30	24
Bal9	Baltic Basin: Darżlubie IG-1, 2925.5 m	35	1	0.7	48	65	0.95	0.13	1.28	0.32	453	135	34	0.37	61
Bal10	Baltic Basin: Darżlubie IG-1, 2935.5 m	30	2	3.0	57	65	5.48	1.47	10.99	0.5	450	200	9	2.88	47
Bal11	Baltic Basin: Darżlubie IG-1, 3015 m	39	4	2.0	50	55	4.09	0.8	9.14	0.43	450	223	11	0.35	91
Bal12	Baltic Basin: Lębork IG-1, 3263.5 m	36	1	4.0	50	59	1.82	0.09	0.21	0.35	478	12	19	0.49	73
Bal13	Baltic Basin: Kościerzyna IG-1, 4384 m	35	2	4.0	52	59	5.25	0.31	0.66	0.42	308	13	8	0.47	91
Bal14	Baltic Basin: Polik IG-1, 4455 m	49	1	1.0	42	47	3.71	0.05	0.15	0.24	399	4	6	0.29	92
Bal15	Baltic Basin: Słupsk IG-1, 4409.7 m	42	4	3.0	39	51	1.21	0.04	0.14	0.24	370	12	20	0.55	55

analysis of randomly oriented powders [30,31]. The total organic carbon (TOC) was analyzed by the LECO method, and the organic matter was characterized by RockEval II by a commercial laboratory (http://www.weatherfordlabs.com).

The 15 Baltic Basin samples were collected from 12 different wells (Fig. 1a) representing the bottom of Silurian strata in northern Poland [32,33]. This organic-rich black shale, mostly containing Type II OM of marine algal source, was deposited in a NW–SE trending foreland basin setting during Late Ordovician time [32]. The rate of basin subsidence during Late Silurian was significantly higher towards the southwest margin [34,35] resulting in differential burial diagenesis of the sediments from E to W (present day depth ranging from 1400 m in E to 5700 m in W). The samples were selected to represent the variation in the OM content and in thermal maturity progressively ranging from immature to overmature, as indicated by decreasing Hydrogen Index (HI) with

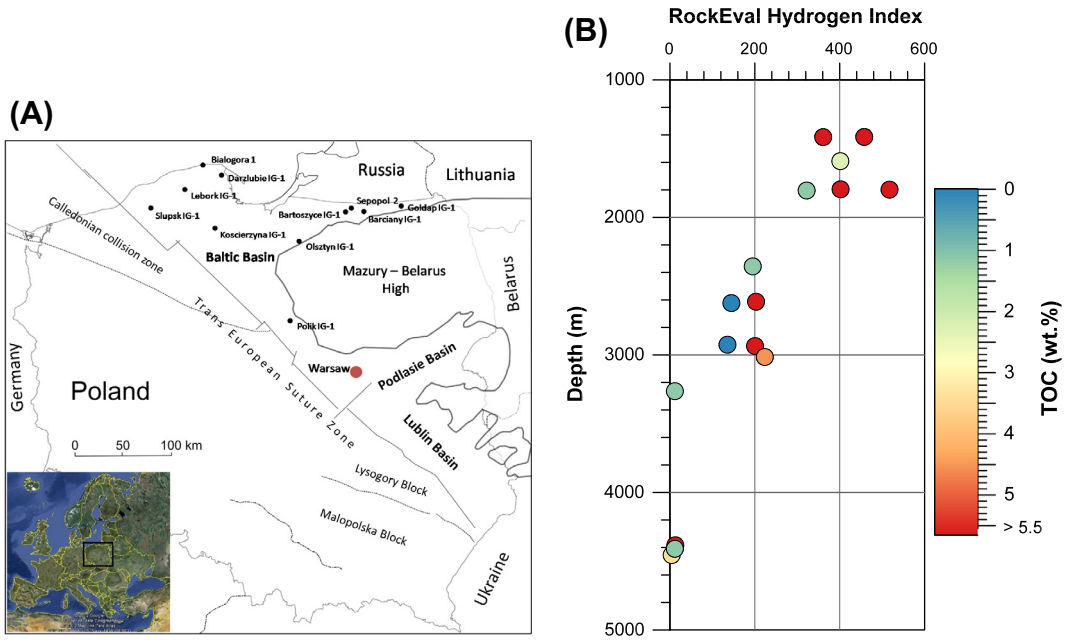

Fig. 1. (A) Map of the Baltic Basin showing the locations of the wells into bottom of Silurian strata (Modified from [34]). (B) RockEval Hydrogen Index (HI) of the Baltic Basin samples plotted as a function of current depth, color coded by their TOC content.

present day depth (Table 1, Fig. 1). This provides an opportunity to track the changes in the pore structure with increasing burial depth and temperature within the same geologic strata, with a common source and a similar marine depositional environment. The mineral composition of the Baltic samples are slightly variable consisting of 24–47 wt.% of total quartz + feldspar, 36–63 wt.% clay minerals represented mostly by mixed-layered illite–smectite (I–S) with <15% of smectite layers [bulk rock total illite + smectite + mixed-layered illite-smectite minerals group (I+S) category; 30–52 wt.%], 1–8 wt.% carbonate minerals (exception Bal8 with 38 wt.% carbonate), and 0.7–6.5 wt.% pyrite (values excluding OM content) (Table 1). The TOC content ranges from 0.52 to 10.33 wt.%. The RockEval HI index varies between 4 and 458 and systematically decreases with current day depth and reflects the maturation trend of the organic matter with increasing burial diagenesis (Table 1 and Fig. 1).

The non-Baltic basin samples have TOC contents ranging from 2.21 to 10.61 wt.% (Table 1). The dominant mineral constituent of these samples is I+S ranging from 20 to 43 wt.% (excluding organic matter). The RockEval HI were consistently low ranging from 5 to 70, indicating overmature OM in these samples. Despite HI being not a direct indicator of thermal maturity, such as vitrinite reflectance, it can be used to assess the relative thermal maturation, especially for the consistent series of the Early Silurian samples where the OM has a marine origin.

2.2. Sample preparation

The samples were crushed in a mortar to pass through a 40 mesh (<420 μm) sieve and split into two mineralogical and chemically equivalent aliquots [36]. One split was treated with sodium hypochlorite solution, to remove OM [37]. Here, 100 ml of a 6% NaOCl solution adjusted to pH of 8.5–9 was added to 5 g of natural sample (<40 mesh) and stirred to keep all the material in suspension. The temperature was then raised to 60–70 °C for 2 h, and the sample was then washed to remove excess salts by centrifugation with deionized (DI) water. This procedure was repeated and the treated samples were dialyzed and dried at 80 °C.

The effectiveness and the impact of OM removal on the composition of the samples were evaluated by TOC measurement and XRD analysis of the samples before and after OM removal. The average OM removal efficiency for 20 samples is 72% ranging from 24% to 96%. The variance in the efficiencies of the OM removal can be influenced by several factors (e.g. [37]). The XRD patterns of the natural and the NaOCl-treated sample (Fig. 2) indicate that the OM removal process also oxidizes and removes pyrite from the samples. All other inorganic phases remain unaffected.

2.3. Pore structure characterization method

Pore structure parameters, including specific surface area (SSA) and pore-size distribution (PSD), of the natural and NaOCl-treated aliquots were measured using the subcritical nitrogen gas adsorption (SGA) at 77 K. About 2–3 g of sample was degassed by heating at 200 °C under vacuum (10 μmHg) prior to the analysis until the out-gassing rates was <2 μmHg/min over a 15 min interval. Measurements in both adsorption and desorption mode were performed over the entire partial pressure range to obtain the adsorption isotherm, with average number of 85 measurement points. SSA for each sample was determined by inversion of the adsorption branch of the isotherm using a modified BET analysis procedure [38]. The micropore volume is estimated using the *t*-plot technique and assuming a Harkins-Jura thickness equation defining the statistical thickness (*t*) of the adsorbed multilayers on pore surfaces. The choice of Harkins-Jura thickness curve was based on closest (0,0) intercept for samples with low SSA samples that likely contain no micropore volume. Pore-size distribution (PSD) is obtained by inverting the adsorption branch of the isotherm using Barett–Joyner–Halenda (BJH) method assuming cylindrical non-connecting pores. The Harkins-Jura thickness equation is used for the multilayer adsorbed volume in the BJH inversion to be consistent with *t*-plot analysis. The relative pore volumes obtained by inversion depends upon the thickness equation used [39] and should be kept consistent to make appropriate comparisons.

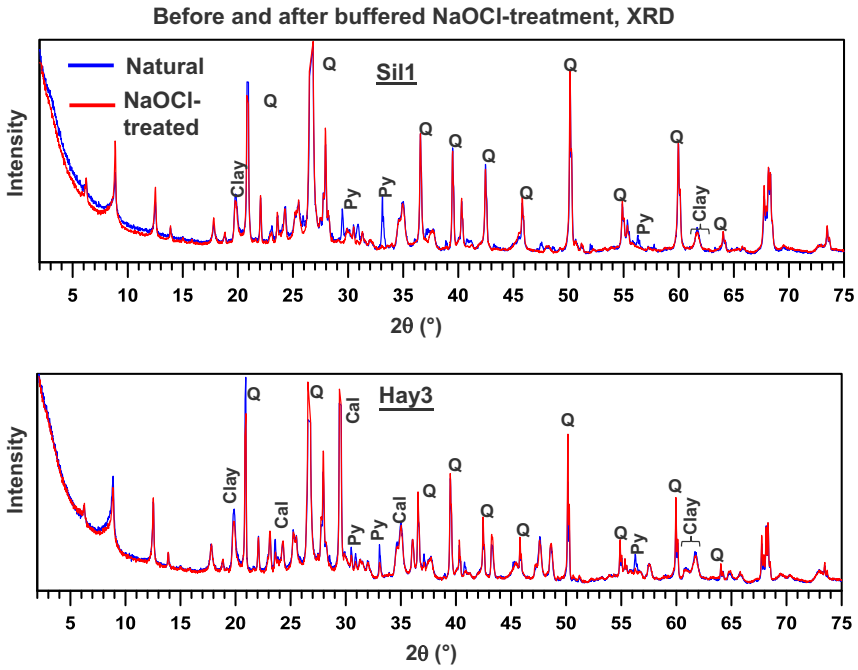

Fig. 2. Bulk XRD patterns of natural (black) and NaOCl-treated (red) aliquots from (top) Sil1 and (bottom) Hay3. Note the lack of pyrite peaks in the NaOCl-treated aliquots. Q = Quartz. Cal = Calcite Py = Pyrite. (For interpretation of the references to color in this figure legend, the reader is referred to the web version of this article.)

3. Results

3.1. Pore structure attributes of the natural samples

The specific surface area of the natural aliquots varies between 1.67 and 56.85 m^2/g. The immature samples with HI > 100 have very low *t*-plot micropore volume (0.000–0.002 cm^3/g), while in the mature samples with HI < 100 the micropore volume varies from 0.002 to 0.023 cm^3/g with average of 0.007 cm^3/g (Table 2, Fig. 3a). The micropore volume of the mature samples with HI < 100 has a positive increase with increasing TOC quantifying the OM content (Fig. 3b).

3.2. Isotherms and pore-size distributions of the natural and NaOCl-treated aliquots

The isotherms of all the samples, both natural and NaOCl-treated aliquots, have a hysteretic isotherm profile with an absence of a plateau at higher $P/P_0 > 0.95$ or the Type IIB profile [40] with either a H3 (no micropores, e.g. Bal1, Fig. 4) or H4 (microporous, e.g. Mar2, Fig. 4) hysteresis pattern. This indicates that these samples are dominated by meso- and macropores and may or may not contain significant micropore volumes. The change in isotherm profile of the samples upon OM removal can be classified into three groups (Fig. 4).

(1) Group A: The NaOCl-treated and natural aliquots have minimal or no difference in the isotherm shape and adsorbed gas content along the entire relative pressure range.
(2) Group B: The adsorbed gas content for the entire relative pressure range increases with OM removal. The hysteresis becomes more prominent in the isotherms of the NaOCl-treated aliquots of some samples (e.g. Bal7).
(3) Group C: The samples have a decrease in the adsorbed gas content at a lower relative pressure range (below $\sim P/P_0 = 0.8$) and an increase in absorbed gas at higher relative pressures in the NaOCl-treated samples compared to the natural aliquots. The degree of hysteresis becomes lower after OM removal compared to the natural aliquots.

These three groups have different patterns of change in the pore size distribution (PSD) plots between 1.7 and 200 nm upon removal of OM matter (Figs. 5–7). After OM removal all the samples have similar bimodal PSD with a prominent mode around the 3 nm pore size. The Group A samples (Bal1, Bal3, Bal4, Bal5 and Bal6) have minimal change in pore volume in the major part of the PSD curve after OM removal, and all the Group A natural and NaOCl-treated samples have a similar bimodal PSD's (Fig. 5). The Group B samples (Bal2, Bal7, Bal8, Bal9, Bal10 and Bal11) have a significant pore volume increase across in the major part of the pore size range after OM removal, especially in the fine mesopore region (2–5 nm). The natural aliquots of Bal 2, Bal 7, Bal10 and Bal11 have a low pore volume in the fine mesopore range (2–5 nm) and do not have the characteristic bimodal pore size distribution with 3 nm modal peak. The natural aliquots of Bal8 and Bal9 have a bimodal PSD with a 3 nm mode, but they have significantly lower pore volumes compared to the NaOCl-treated aliquots (Fig. 6). The Group C, samples Sil1, Hay1, Hay2, Hay3, Pal1, Pal2, Mar1, Mar2, Bal13 and Bal14, have a significant reduction in the pore volume network below the ~5.0 nm pore size, and a significant increase in pore volume for larger pore size diameters (Fig. 7). The efficiency of the OM removal process does not show any systematic correlation with the observed changes in the pore-size distributions.

3.3. Quantification of relative OM hosted pore volume

The changes observed in the pore-structure attributes after OM removal can be quantified to understand the relative significance of OM hosted porosity and clay aggregate hosted porosity in natural mudrocks along with correlation to thermal maturity. For this purpose, a pore size boundary of less than 5 nm was chosen. Porosity in clay aggregates has characteristic PSD populations between 2 and 5 nm with a ~3 nm maxima. The micropores

Table 2
Pore-structure attributes of the investigated samples obtained from N_2 gas adsorption. SSA = specific surface area using modified BET method [38]; $V\mu$ = Micropore (<2 nm) volume using *t*-plot with Harkins-Jura thickness equations; Vp_{2-5nm} = Total pore volume between 2 and 5 nm pores size obtained from BJH inversion with Harkins-Jura thickness equation; $Vp_{<5nm} = V\mu + Vp_{2-5nm}$.

Sample	Natural Aliquot				NaOCL-treated (OM removed) Aliquot				Proportion of pores <5 nm	
	SSA (m^2/g)	$V\mu$ (cm^3/g)	Vp_{2-5nm} (cm^3/g)	$Vp_{<5nm}$ (cm^3/g)	SSA (m^2/g)	$V\mu$ (cm^3/g)	Vp_{2-5nm} (cm^3/g)	$Vp_{<5nm}$ (cm^3/g)	Clay Hosted % $Vp_{<5m}$	OM Hosted % $Vp_{<5m}$
Eastern Europe Silurian shale										
Sil1	21.16	0.007	0.003	0.010	10.25	0.001	0.003	0.003	33	67
Haynesville										
Hay1	26.22	0.007	0.005	0.012	9.54	0.000	0.003	0.003	74	26
Hay2	15.45	0.003	0.004	0.007	16.30	0.000	0.005	0.005	23	77
Hay3	18.65	0.003	0.005	0.008	14.07	0.000	0.004	0.004	55	45
North American Paleozoic shale										
Pal1	9.76	0.002	0.002	0.004	13.03	0.000	0.004	0.004	–––	–––
Pal2	17.64	0.004	0.004	0.008	10.60	0.000	0.003	0.003	37	63
Marcellus										
Mar1	56.85	0.023	0.007	0.030	15.32	0.001	0.005	0.006	21	79
Mar2	34.25	0.020	0.009	0.030	13.03	0.000	0.004	0.004	14	86
Baltic basin										
Bal1	21.96	0.000	0.008	0.008	23.43	0.001	0.008	0.008	–––	–––
Bal2	12.33	0.000	0.003	0.003	27.90	0.004	0.008	0.012	–––	–––
Bal3	24.98	0.001	0.009	0.010	28.32	0.002	0.009	0.011	–––	–––
Bal4	16.70	0.001	0.007	0.007	20.51	0.002	0.007	0.009	–––	–––
Bal5	27.10	0.001	0.010	0.011	26.53	0.001	0.008	0.009	–––	–––
Bal6	17.23	0.000	0.006	0.006	20.10	0.000	0.006	0.006	–––	–––
Bal7	1.67	0.000	0.000	0.000	9.30	0.001	0.003	0.004	–––	–––
Bal8	4.29	0.000	0.001	0.002	7.66	0.001	0.002	0.004	–––	–––
Bal9	8.45	0.002	0.003	0.005	12.90	0.003	0.004	0.006	–––	–––
Bal10	2.56	0.000	0.001	0.001	5.74	0.000	0.002	0.002	–––	–––
Bal11	12.10	0.000	0.003	0.003	21.56	0.002	0.006	0.008	–––	–––
Bal12	17.02	0.005	0.005	0.010	14.66	0.001	0.003	0.004	39	61
Bal13	19.36	0.005	0.004	0.009	15.62	0.002	0.004	0.006	70	30
Bal14	11.20	0.003	0.003	0.006	9.58	0.001	0.002	0.003	47	53
Bal15	7.12	0.002	0.001	0.003	9.23	0.000	0.003	0.003	76	24

(<2 nm) are also important as they have significant contribution in these samples (Fig. 3). Combining the pronounced PSD populations between 2 and 5 nm obtained from BJH inversion, with the micropore (<2 nm) volume obtained from the *t*-plot calculation into one volume population ($Vp_{<5nm}$) is thus justified. Quantitative evaluation of the total pore volume hosted in clay mineral aggregates and OM in the mature samples is possible by comparing the cumulative pore-size distribution between the NaOCl-treated and natural aliquots. The natural samples will have both open clay-hosted porosity and OM porosity, while the NaOCl-treated samples will ideally only have clay aggregate or other inorganic hosted porosity. The difference in pore volumes between these two aliquots will give an estimate of the OM hosted porosity (Fig. 8).

The $Vp_{<5nm}$ of the natural aliquots ranges from 0.000 to 0.030 cm^3/g while after OM removal it varies from 0.002 to 0.012 cm^3/g (Table 2). While the natural $Vp_{<5nm}$ does not have a linear trend with HI (Fig. 9a), the change in $Vp_{<5nm}$ ($\Delta Vp_{<5nm}$) after OM removal has a well-defined boundary near HI of 100 where below this value only positive $Vp_{<5nm}$ values are observed with these higher maturity samples (Fig. 9b). The less mature samples with HI > 100, except Bal5, have either no change or an increase in micropore volume after OM removal. The mature samples (HI < 100), except Pal1, all have a significant decrease in micropore volume with OM removal (Fig. 9b). Comparison of $Vp_{<5nm}$ for the natural samples containing both clay-hosted and OM hosted pores, and the NaOCl-treated samples with only clay-hosted pores, indicates that the OM-hosted pores account for at least 26–77% of the total pore volume within the <5 nm pore-size interval (Table 2). Such an estimation is possible only for the samples where the $Vp_{<5nm}$ decreases upon OM removal.

4. Discussion

4.1. Mudrock nano structure

These results comparing PSD's before and after OM removal clearly demonstrate the organic fabric and influence of OM in the nanostructure of mudrocks. The most striking similarity between all the samples is the bimodal PSD with a modal peak around 3 nm obtained from the NaOCl-treated aliquots, which is characteristic of the illite + smectite clay hosted porosity [26]. This finding suggests that the clay aggregate nanostructure is one of the fundamental textural controls of mudrocks at the nanometer scale. The three different groups and types of PSD changes observed in this study highlight the nm-scale heterogeneity in the mudrock texture and the respective arrangement of clay minerals and OM.

The samples with no significant change in PSD distribution after OM removal (Group A, Fig. 5) have a bimodal PSD with a prominent 3 nm modal peak in the native state (natural aliquots). This indicates, that even though there is a significant amount of OM, the majority of clay hosted porosity in the untreated samples is still open in the <2 nm to ~200 nm interval covered by the SGA-N_2 analysis. The lack of a significant change in the PSD after OM removal indicates that the OM in these samples is texturally distributed at a scale >200 nm and the OM itself does not have any fine-scale open porosity. The OM must be present either as discrete particles, or as laminations significantly larger than 200 nm. That there is OM in particles >200 nm is confirmed by mercury intrusion porosimetry of natural and NaOCl-treated aliquots of the same samples and will be presented in a future study.

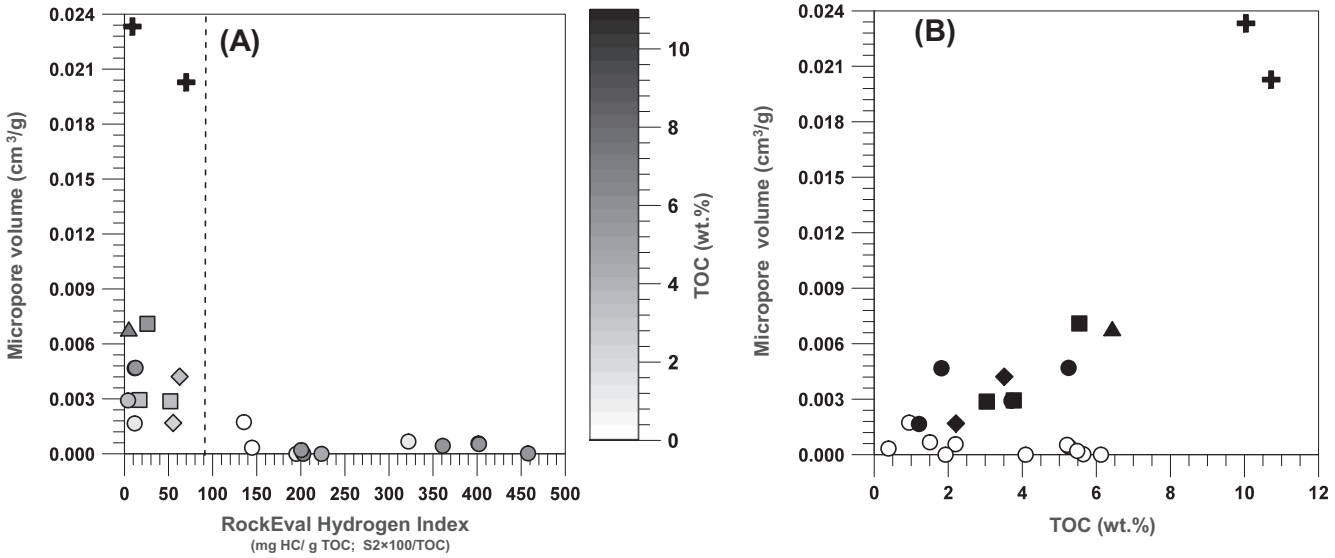

Fig. 3. (A) Micropore volume of the natural aliquots of the samples as a function of thermal maturity as indicated by RockEval Hydrogen Index. The samples are color coded by their TOC content. (B) Micropore volume of the natural samples. The black color indicates mature samples with HI < 100 while the white color indicates immature samples with HI > 100. Circles: Baltic Basin; Triangle: Eastern European Silurian Shale; Diamonds: North American Palaeozoic Shale; Squares: Haynesville Shale; Plus: Marcellus Shale.

The samples of Group B (Fig. 6) have a consistent increase in pore volume across the entire SGA-N_2 pore-size range, especially in the fine mesopore region (2–5 nm). The natural aliquots that have abundant TOC in this group (Bal2, Bal7, Bal10 and Bal11) have especially low pore volume in the 2–5 nm mesopore range, and do not have the characteristics bimodal pore size distribution with a 3 nm modal peak. Removal of OM results in increased pore volume and the 3 nm modal peak becomes evident. In these samples, the OM occurs as pore-filling material within the clay nanostructure and the loss of OM resulted in exposure of clay-hosted small diameter porosity. The TOC-poor samples of this group have a bimodal PSD with a 3 nm peak in the natural samples, but they show an increase in pore volume along entire PSD range after OM removal. There was not enough OM to fill the entire clay aggregate framework, but it occludes some of the clay aggregate porosity which opens after OM removal. A similar type of organic matter filling within the mesoporous structure of clay mineral aggregates was documented in immature oil shales [15,16,20–22,41], and ocean floor sediments and soils [17–19,42]. Kuila et al. [39]observed similar OM pore filling within the clay nanostructures in Niobrara Formation samples from Colorado. This pattern of OM and clay mineral interaction may be responsible for the enhanced preservation of OM in marine sediment [19].

Group C samples have a reduced pore volume network below the ~5.0 nm pore size and a strong increase in pore volume for larger pore diameters after OM removal (Fig. 7). The increase in pore volume at larger pore diameters (above 5–10 nm) in the Group C samples is due to removal of pore-filling OM from the mesopores within clay mineral aggregates, similar to the Group B samples. However, the reduction in pore volume at smaller pore diameters (<5 nm) indicates that the OM matter itself is the host of fine mesopores and micropores within the OM matrix, both of which are destroyed when the OM is removed. This observation is consistent with the overall higher micropore volume in the natural aliquots of Group C samples compared to that of the Group B samples. These data prove the presence of micropores and fine mesopores (<5 nm) within the OM of the Group C samples, while the OM in Group B samples is probably non-porous or macroporous with <200 nm pores. The presence of larger pores in OM of Group C is also possible, but it is masked by the dominant effect of opening pores within clay aggregates after OM removal. An example FESEM image (Fig. 10) from a similar Eastern Europe Silurian shale sample shows a representative textural arrangement where the OM hosts a 'sponge like' [2] pore network completely filling the space formed by the arrangement of the phyllosilicate aggregates. A similar textural relationship between the clay nanostructure and porous OM in other mudrocks was reported by Schieber [12] and Milliken et al. [2]. Although in the Group C samples the OM may still occlude pores in the clay matrix that then open after OM removal, the decrease of the micro- and fine mesopore volume from nanoporous OM removal is the overwhelming effect.

The three different groups of PSD's and the changes observed after OM removal highlight the inherent heterogeneity at the nanometer scale textural arrangement of clay mineral pore surfaces and OM. There is no obvious correlation between mineral composition and OM content that can be associated with any of these three groups of PSD's. The change in PSD's observed after OM removal clearly shows that there is a significant variety of OM and inorganic textural arrangements that can dominant in a sample. However, these data do not provide any detailed information about the homogeneity or heterogeneity of OM porosity within a single sample.

4.2. Relation with maturity

The data in this study indicate that there is a clear correlation between pore structure and the thermal maturity of the samples indicated both by burial depth for the Baltic samples (Fig. 1), and by the RockEval hydrogen index values for the Baltic samples as well as the other formations (Fig. 9). The $Vp_{<5nm}$ (Fig. 9b) and meso and fine macropore (Figs. 5 and 6) of the immature samples, with HI > 100, increases or is unchanged upon OM removal, irrespective of their TOC content. The $Vp_{<5nm}$ and the fine mesopore volume in the natural aliquots of these samples are attributed to open clay-hosted porosity. This indicates the non-porous or macroporous (with >200 nm pores) nature of OM in these samples. The absence of open nanopores in the OM of the low-maturity samples suggests either the absence of primary OM porosity, or the primary porosity is completely clogged by remobilized OM during early diagenesis (like bitumen). Previous work on the physical and chemical

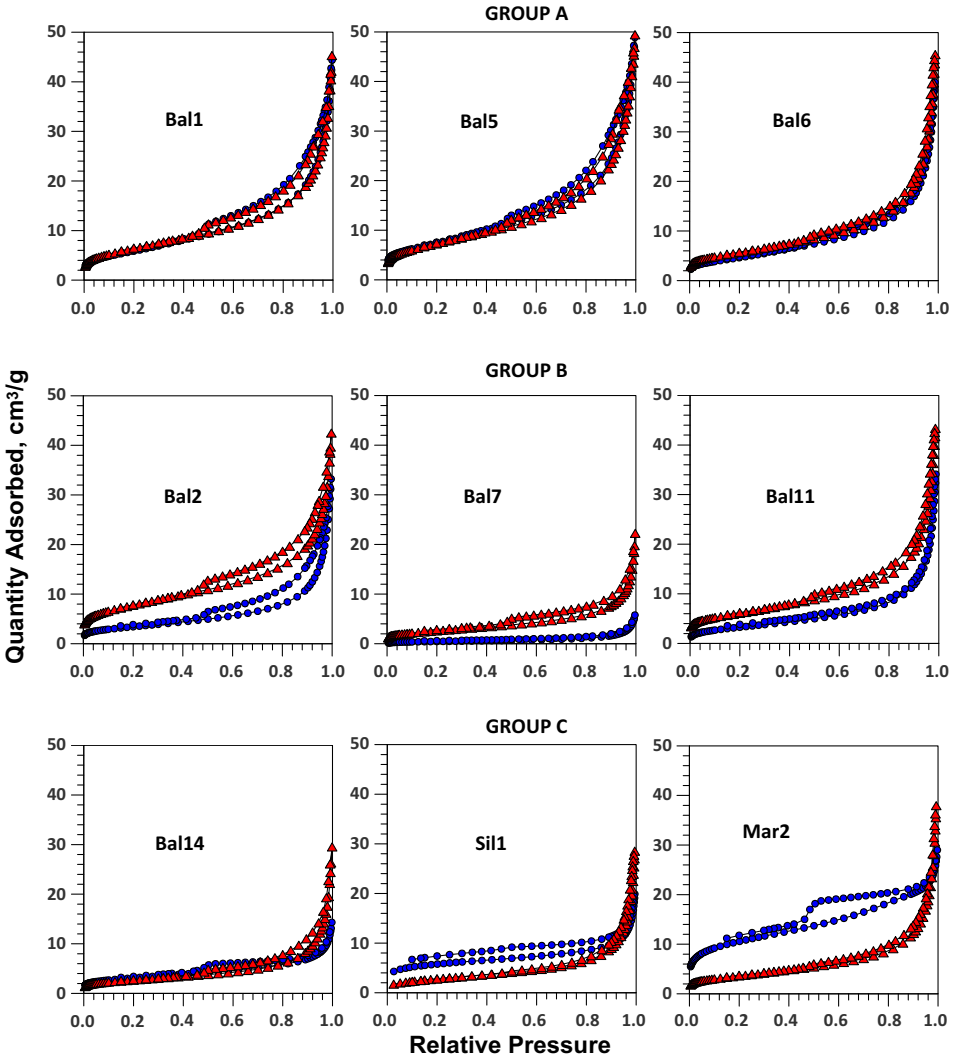

Fig. 4. Representative isotherms of the natural (blue circles) and NaOCl-treated (red triangles) aliquots of the samples. The samples can be classified into three groups depending upon the relative isotherm patterns between the natural and NaOCl-treated aliquots (detailed explanation in the text). (For interpretation of the references to color in this figure legend, the reader is referred to the web version of this article.)

changes of immature OM from the Green River Formation, suggest that with increasing thermal maturity the original organic matter decomposes in successive stages producing bitumen, immiscible oil, followed by gas and pyrobitumen [43]. Schnackenberg and Prien [44] and Johnson et al. [45] reported an intermediate stage where the kerogen softens to a rubber- like material or 'rubberoid', prior to generation of hydrocarbons. Experimental pore-structure evolution in oil shales showed a decrease in total pore volume of oil shales on heating up to 400 °C [16,20–22]. This observation was attributed to the pore blockage by the remobilized bitumen upon cooling into the previously open pores [11,16,20].

The mature samples with HI < 100 have consistently higher micropore volumes than the immature samples (Fig. 3a). These mature samples have a significant decrease in $Vp_{<5nm}$ after OM removal indicating that the majority of the micro- and fine mesopores present in the natural sample is associated with OM (Fig. 9b). This is consistent with the observation that all the samples in Group C have low HI (Fig. 7). The only exception is Pal1 which does not show any change in $Vp_{<5nm}$ after OM removal, but does have a change in the plotted PSD data (Fig. 7) indicating a significant pore volume with <3 nm diameters in the native state was destroyed after OM removal. The open porosity in the OM may be a result of expulsion of hydrocarbon which was clogging the primary porosity in OM or porosity was somehow created by thermochemical changes, or a combination of both. As discussed previously, HI is a relative maturity indicator and, the exact thermally maturity conditions beyond which OM hosted porosity starts developing cannot be established. However, based on these data OM porosity appears to develop in a punctuated or episodic manner after a thermal threshold is reached.

4.3. Quantification of relative OM hosted pore volume

The quantitative comparison of $Vp_{<5nm}$ between the NaOCl-treated and natural aliquots gives an estimate of the minimum contribution that the fine pores hosted in OM make to the total $Vp_{<5nm}$ pore volume. The positive $\Delta Vp_{<5nm}$ values in the mature samples after OM removal can be treated as an indication of the OM hosted pore volume up to a 5 nm diameter size range. However, OM removal not only destroys pores associated with OM, but will also open additional pores within clay mineral aggregates in the <5 nm size range, which was otherwise occupied by OM in the natural samples. Therefore, the $Vp_{<5nm}$ clay-hosted porosity measured in the NaOCl-treated sample is greater than that which is present in the natural sample. Thus, the calculated relative volume of OM-hosted porosity will be lower than actual and should

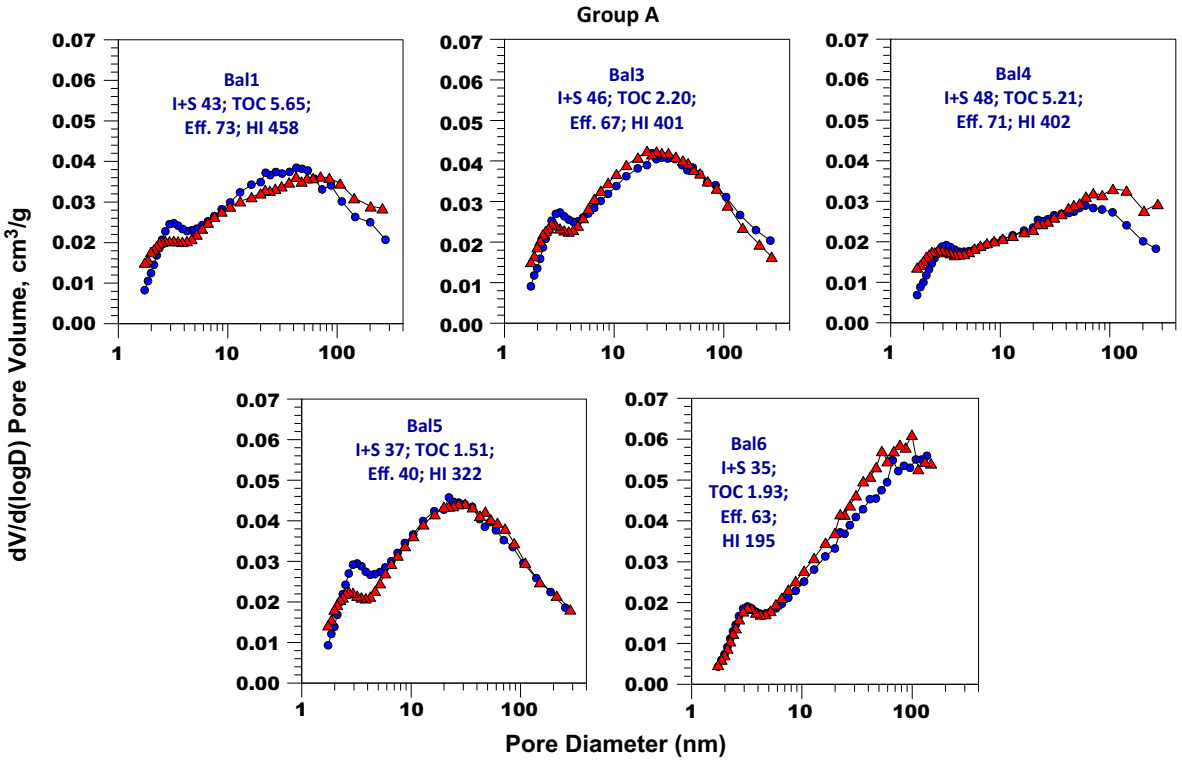

Fig. 5. Pore size distribution of samples showing minimal changes in pore volume along the entire pore size range after OM removal. Blue circles represent the natural aliquot while the red triangles are the OM removed aliquot. I+S = illite + smectite clay group in wt.%; TOC = Total Organic Carbon in wt%; Eff. = OM removal efficiency in %; HI = Hydrogen Index in mg HC/g TOC. (For interpretation of the references to color in this figure legend, the reader is referred to the web version of this article.)

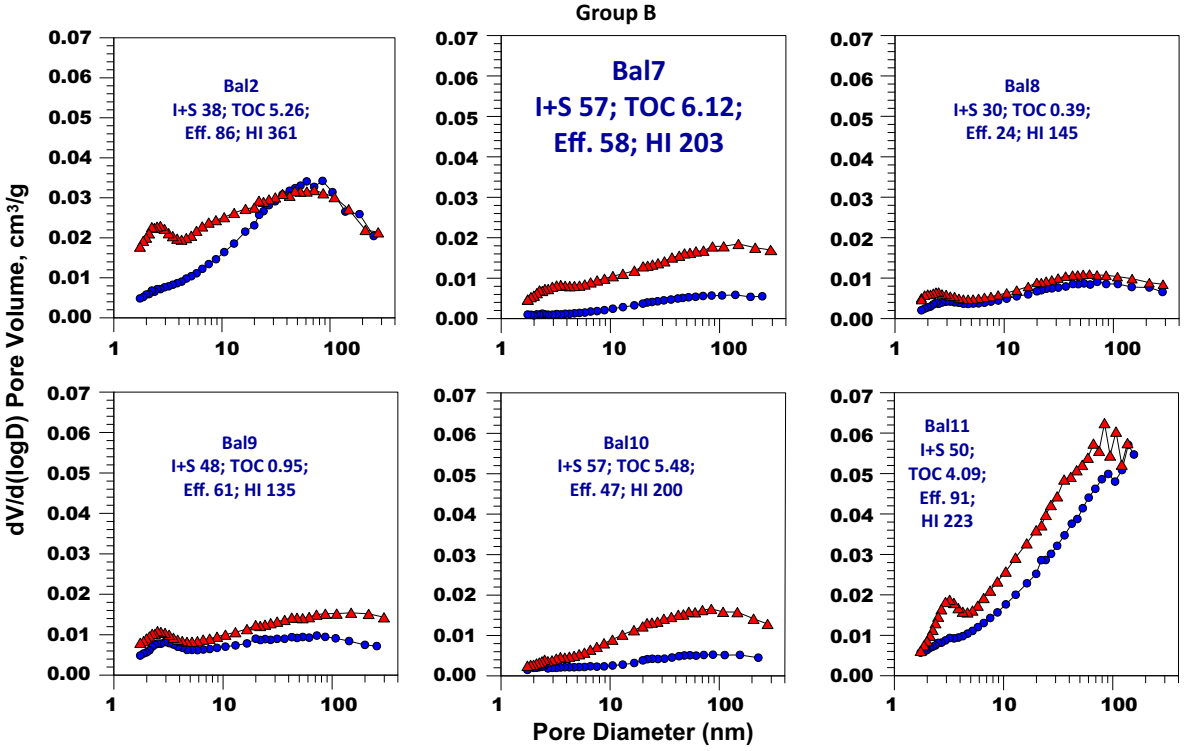

Fig. 6. Pore size distribution of samples showing significant pore volume increase across in the major part of the pore size range upon OM removal, especially in the fine mesopore region (<10 nm). Blue circles represents the natural aliquot while the red triangles are the OM removed aliquot. I+S = illite + smectite clay group in wt.%; TOC = Total Organic Carbon in wt%; Eff. = OM removal efficiency in %; HI = Hydrogen Index in mg HC/g TOC. (For interpretation of the references to color in this figure legend, the reader is referred to the web version of this article.)

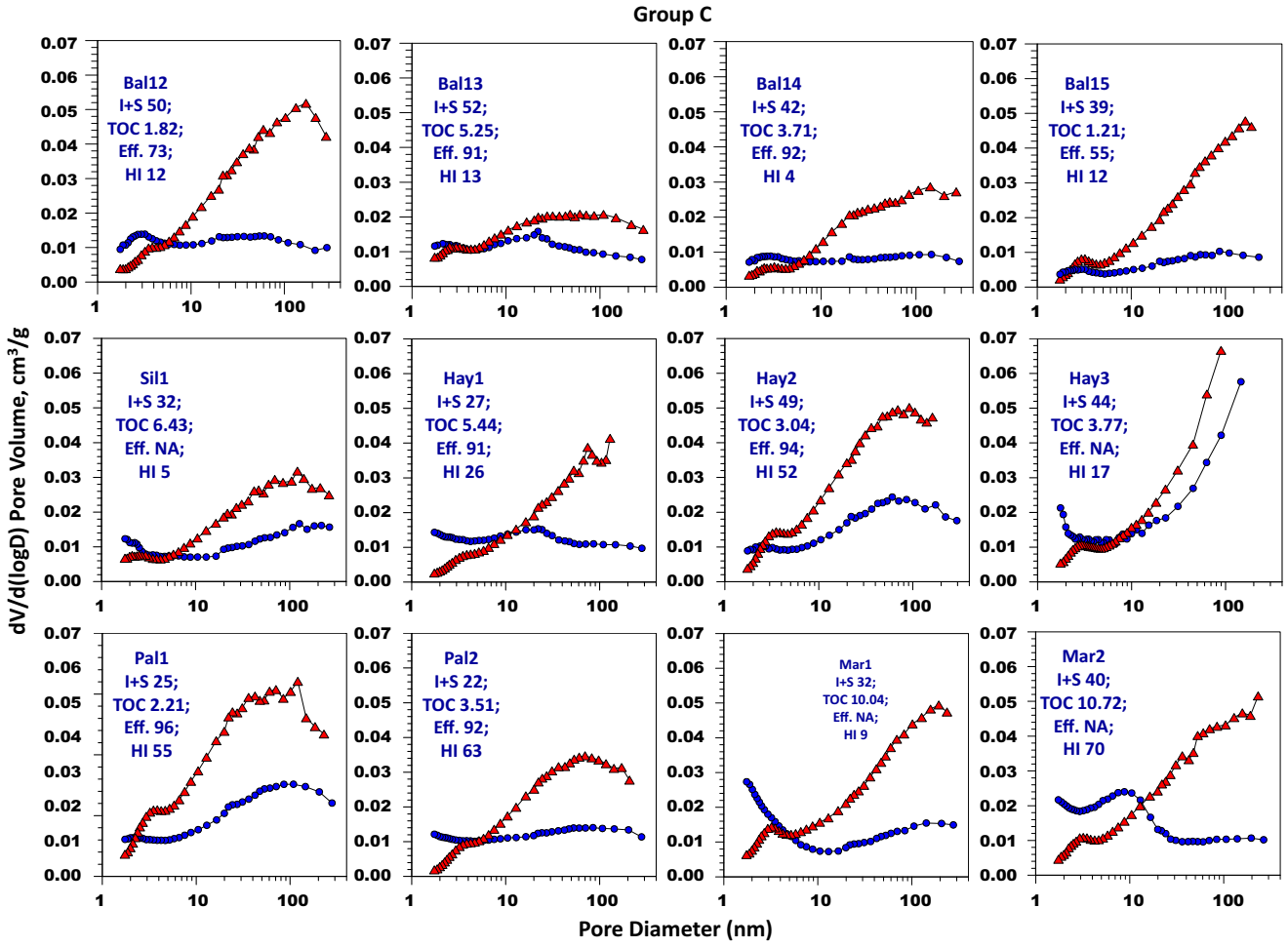

Fig. 7. Pore size distribution of samples showing significant pore volume decrease below 5 nm pore size upon OM removal. Blue circles represents the natural aliquot while the red triangles are the OM removed aliquot. I+S = illite + smectite clay group in wt.%; TOC = Total Organic Carbon in wt%; Eff. = OM removal efficiency in %; HI = Hydrogen Index in mg HC/g TOC. (For interpretation of the references to color in this figure legend, the reader is referred to the web version of this article.)

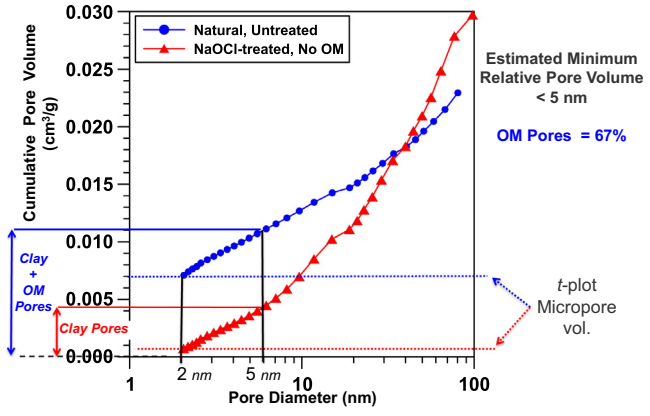

Fig. 8. Comparison of cumulative pore size distribution of natural (circle) and NaOCl-treated (triangle) aliquots of the Eastern European Silurian Shale (Sil1). The cumulative pore volume between 2 and 100 nm is obtained from BJH inversion and the micropore volume (<2 nm) is obtained from *t*-plot. The difference in pore volume in the <5 nm pore size between the natural and NaOCl-treated aliquot (No OM) is used to estimate the relative volume of clay-hosted and OM hosted porosity in the natural samples (see text for detailed explanation).

be treated as the minimum possible OM-hosted $Vp_{<5nm}$ pore volume. Milliken et al. [2] suggested that the percentage of pore volumes in the Marcellus Formation mudrocks assigned to the OM-hosted pores that are below FESEM microscopy resolution (4–7 nm) are 58–98% of the total porosity. Given the limitation of FESEM images, the experimental technique presented in this study provides a missing link between FESEM data and the evolution of OM-hosted porosity upon thermal maturation.

The conversion of the $\Delta Vp_{<5nm}$, corresponding to OM-hosted fine porosity, to porosity values (% bulk volume) is not straight forward as the grain density of the natural and NaOCl-treated aliquots will be different. The grain densities were estimated from the QXRD results for the NaOCl–treated samples, and the grain density of the natural samples was calculated assuming different OM densities and assuming 83 wt.% carbon content within the OM (Table 3). The OM hosted <5 nm porosity can be up to 5.42–5.93% of total bulk volume in the highest OM content samples from the Marcellus Formation. Given the total bulk volume porosity in the range of 5.0–8.7% measured for the TOC-rich Marcellus samples by Milliken et al. [2], measurements from this study confirm the suggestion that the majority of bulk volume porosity can occur as OM-host pores below the detection limit of modern FESEM instruments [2]. An additional 1–2% of total porosity with pore dimension <5 nm occurs within mineral-hosted pores. In all other samples measured in the present study the equivalent total porosity present as pores <5 nm, is 1–2% of bulk volume (BV). Because the total porosity in typical OM-rich shale is 3–10% BV, the fraction of porosity not detectable by FESEM imaging accounts for 10–70% of the total porosity. However, it should be noted the pore volumes obtained from the BJH inversion used in this study can differ

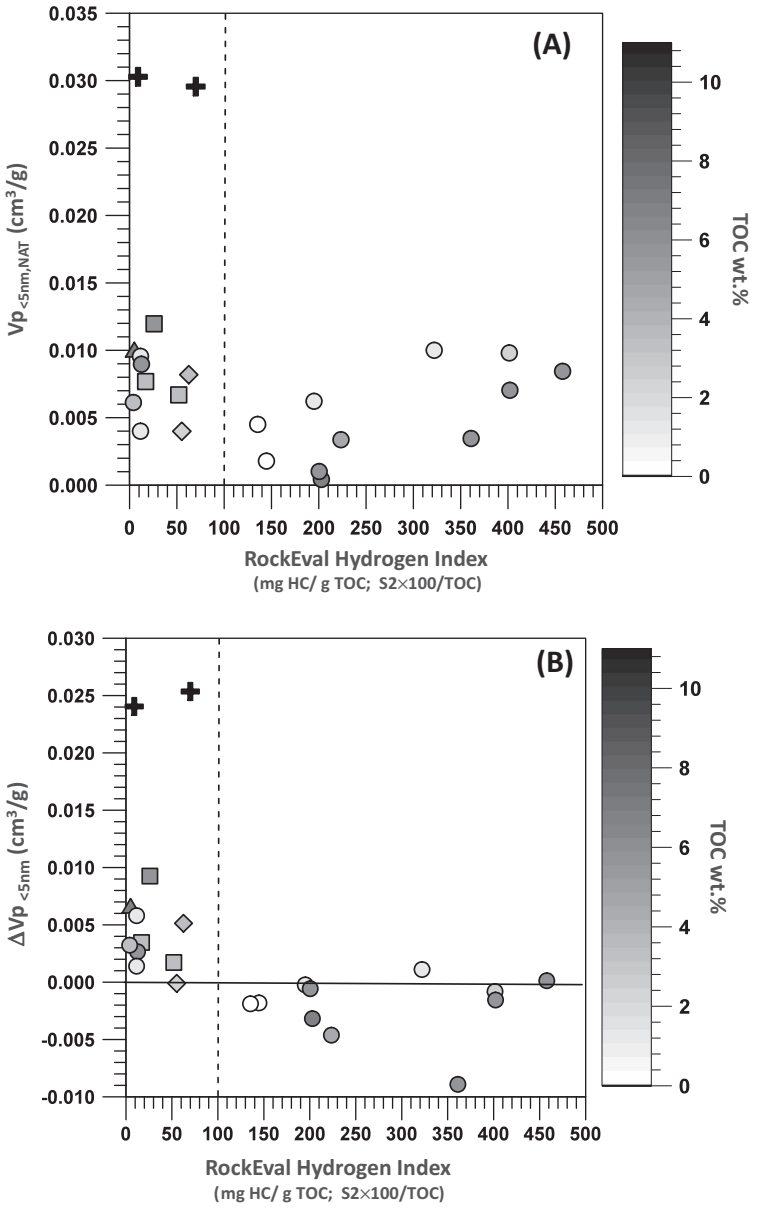

Fig. 9. (A) $Vp_{<5nm}$ of the natural aliquots of the samples plotted against thermal maturity as indicated by RockEval Hydrogen Index. (B) Difference in $Vp_{<5nm}$ between the natural and the NaOCl-treated aliquots ($\Delta Vp_{<5nm}$) of the samples plotted against maturity. The samples are color coded by their TOC content. Circles: Baltic Basin; Triangle: Eastern European Silurian Shale; Diamonds: North American Palaeozoic Shale; Squares: Haynesville Shale; Plus: Marcellus Shale.

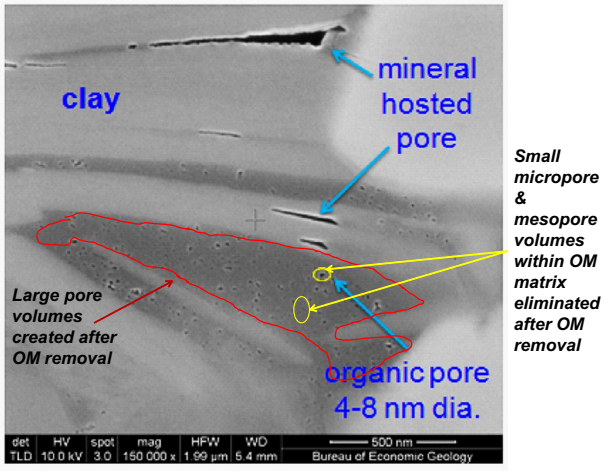

Fig. 10. FESEM image of ion milled sample from Eastern European Silurian Gas Shale.

depending upon the inversion assumptions up to 40% (relative) depending upon choice of inversion parameters [39].

The PSD data obtained for all the samples in this study indicates that both clay and OM hosted porosity contribute to $Vp_{<5nm}$. In the mature samples, with HI < 100, $\Delta Vp_{<5nm}$ increases with TOC, regardless the samples' origin and age (Fig. 11a). Although the correlation is scattered, the tendency is clear. A similar relationship is observed in the micropore (<2 nm) volume change ($\Delta V\mu$) (Fig. 11b). The change in the pore volumes should ideally be correlated with the change in TOC (ΔTOC) content to account for the variance in OM removal efficiency. However in this study, OM removal efficiency does not show any significant control on the pore volume changes (Fig. 11a). The correlation between TOC and $Vp_{<5nm}$ is consistent with the previously reported correlation between OM and total porosity in gas shales [1,2]. The observed positive relationship of $\Delta Vp_{<5nm}$ and TOC from this mature mudrock sample set from different locations suggests a common mechanism in the development of OM porosity. A possible mechanism

Table 3
Estimated OM fine porosity (OM $\varphi_{<5nm}$) from the measured fine-scale pore volume ($Vp_{<5nm}$)and estimated grain densities. Maximum clay-hosted fine porosity (Clay $\varphi_{<5nm}$) estimated from measured pore volume from the NaOCl treated aliquot. The grain density (GD) of the mineral fractions were obtained from QXRD. Three different density of OM (ρ_{OM}) is assumed to show the variation in the estimation.

Sample	TOC	QXRD GD (Mineral fraction)	Whole rock GD			$Vp_{<5nm}$ NaOCl-treated aliquot	Clay $\varphi_{<5nm}$	$Vp_{<5nm}$ Natural aliquot	Clay + OM $\varphi_{<5nm}$			OM $\varphi_{<5nm}$
			ρ_{OM} = 1.1	ρ_{OM} = 1.3	ρ_{OM} = 1.5				ρ_{OM} = 1.1	ρ_{OM} = 1.3	ρ_{OM} = 1.5	
	(wt.%)	(g/cm^3)	(g/cm^3)	(g/cm^3)	(g/cm^3)	(cm^3/g)	% BV	(cm^3/g)	% BV	% BV	% BV	% BV
Eastern Europe Silurian shale												
Sil1	6.43	2.766	2.475	2.543	2.595	0.003	0.93	0.010	2.43	2.49	2.54	1.50–1.62
Haynesville												
Hay1	5.54	2.804	2.540	2.602	2.649	0.003	0.75	0.012	2.95	3.02	3.07	2.20–2.32
Hay2	3.04	2.781	2.635	2.671	2.698	0.005	1.37	0.007	1.73	1.76	1.77	0.37–0.41
Hay3	3.77	2.773	2.596	2.639	2.672	0.004	1.16	0.008	1.95	1.99	2.01	0.80–0.85
North American Paleozoic shale												
Pal1	2.21	2.802	2.691	2.718	2.738	0.004	1.14	0.004	1.06	1.07	1.08	–––
Pal2	3.51	2.762	2.596	2.636	2.648	0.003	0.84	0.008	2.08	2.11	2.12	1.24–1.29
Marcellus												
Mar1	10.04	2.972	2.465	2.572	2.657	0.006	1.82	0.030	6.95	7.23	7.45	5.13–5.63
Mar2	10.72	2.920	2.406	2.515	2.602	0.004	1.21	0.030	6.64	6.92	7.14	5.42–5.93
Baltic basin												
Bal1	5.65	2.750	2.496	2.556	2.603	0.008	2.24	0.008	2.06	2.11	2.15	–––
Bal2	5.26	2.786	2.540	2.598	2.643	0.012	3.33	0.003	0.87	0.89	0.91	–––
Bal3	2.20	2.785	2.677	2.704	2.723	0.011	2.87	0.010	2.56	2.58	2.60	–––
Bal4	5.21	2.775	2.533	2.590	2.634	0.009	2.33	0.007	1.75	1.79	1.82	–––
Bal5	1.51	2.780	2.705	2.724	2.738	0.009	2.43	0.011	2.78	2.80	2.82	–––
Bal6	1.93	2.818	2.719	2.743	2.761	0.006	1.79	0.006	1.66	1.68	1.69	–––
Bal7	6.12	2.814	2.524	2.592	2.644	0.004	1.00	0.000	0.11	0.11	0.11	–––
Bal8	0.39	2.762	2.742	2.747	2.751	0.004	0.98	0.002	0.49	0.49	0.49	–––
Bal9	0.95	2.795	2.747	2.759	2.768	0.006	1.76	0.005	1.22	1.23	1.23	–––
Bal10	5.48	2.819	2.555	2.617	2.664	0.002	0.44	0.001	0.26	0.26	0.27	–––
Bal11	4.09	2.788	2.592	2.639	2.675	0.008	2.18	0.003	0.87	0.88	0.89	–––
Bal12	1.82	2.824	2.730	2.761	2.770	0.004	1.05	0.010	2.54	2.57	2.58	1.49–1.53
Bal13	5.25	2.828	2.573	2.633	2.678	0.006	1.75	0.009	2.25	2.31	2.35	0.50–0.59
Bal14	3.71	2.760	2.585	2.628	2.660	0.003	0.79	0.006	1.56	1.58	1.60	0.76–0.81
Bal15	1.21	2.805	2.743	2.758	2.770	0.003	0.73	0.003	0.93	0.94	0.94	0.20–0.21

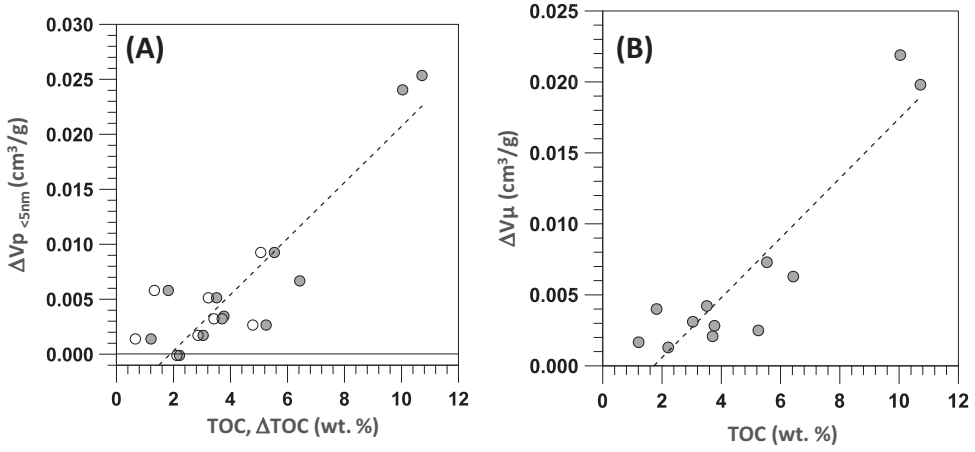

Fig. 11. (A) $\Delta Vp_{<5nm}$ plotted versus TOC and ΔTOC values for the mature samples (HI < 100). The solid circles indicate the TOC of the natural samples. Hollow circles indicate the ΔTOC values (B) Change in micropore volume ($\Delta V\mu$) upon OM removal plotted versus TOC of the mature samples (HI < 100).

may be that bubbles nucleate homogenously within soft OM during hydrocarbon expulsion, which would produce a similar porosity fraction per OM mass unit in different mudrocks. However, this study does not provide information about larger pores that were frequently reported within OM fractions and are considered as produced by different mechanisms [2]. Milliken et al. [2] reported a negative correlation between FESEM detectable OM porosity (<5 nm) with OM content suggesting several other mechanisms may also be responsible for OM porosity evolution.

5. Implication to absorbed gas potential of mature mudrocks

Quantification of OM-hosted micropores and fine mesopore volumes (2–5 nm) in thermally mature mudrocks has widespread implications in understanding gas storage capacity and production potential. A significant amount of natural gas stored in these formations is adsorbed. This adsorption phenomenon is a surface area controlled process and the amount of gas adsorbed depends on both the total surface area and the surface energy of the pores.

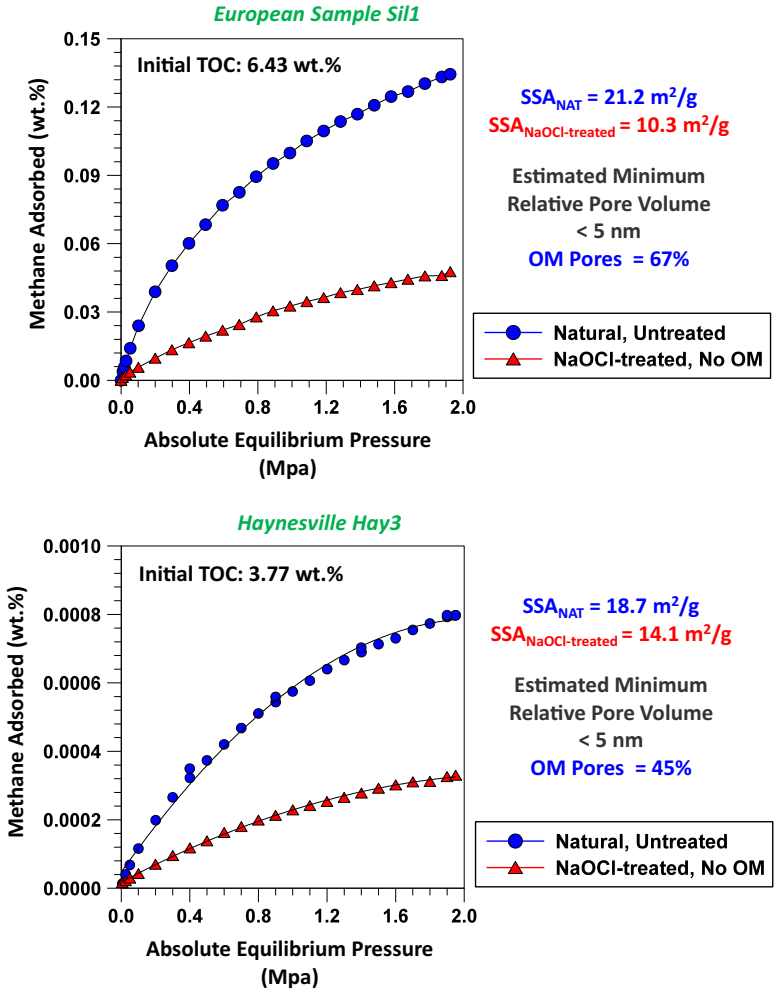

Fig. 12. Comparison of supercritical methane adsorption (at 35 °C) between the natural and NaOCl-treated (No OM) aliquots of samples (top) Sil1 and (bottom) Hay3 highlighting the importance of OM in adsorbed methane gas quantities of shale pays. The pore structure attributes are obtained from low pressure nitrogen gas adsorption measurements (Table 2).

The greatest amount of pore surface area is associated with the micropores and fine mesopores even though it may be a minor proportion of total pore volume. Moreover, whether these micropore and mesopore networks exist either exclusively within the organic matter or as pore systems in the inorganic components is also critical to production due to the difference in surface energy between the two types of components [7,29]. The quantitative results on OM hosted porosity obtained from this study can be directly used to model the adsorption and desorption behavior under reservoir conditions.

In order to show the contrast in adsorption behavior after OM removal a high pressure methane adsorption experiment was conducted on two samples. In this experiment an IGA Gas Sorption Analyzer (Hiden Analytical Inc.) was used to measure the adsorption isotherms of methane at 35 °C on the natural and NaOCl-treated aliquots (Fig. 12) of Sil1 and Hay3 up 2.0 Mpa pressure. Equilibrium uptake at different pressures is determined by quantifying weight gain or loss after pressure change. Comparison of adsorption isotherm between the natural and the NaOCl-treated aliquots indicate that methane adsorption is strongly controlled by the presence of OM. Both the NaOCl-treated samples, regardless their origin and different absolute quantity of adsorbed methane, show much lower methane adsorption than the natural samples, indicating methane has a greater affinity for organic matter than for illite–smectite and other inorganic surfaces or pore systems hosted in clay aggregates. The difference in methane adsorption before and after OM removal roughly correlates to the relative proportion of $Vp_{<5nm}$ contribution provided by OM and clay texture. Noticeably, the network of pores with dimension <5 nm corresponds exclusively to the adsorbed gas [46], therefore, the observed difference in methane adsorption is due to the gas adsorbed in a fine network. Since both OM and clay contribute to the total SSA and micropore-fine mesopore volume in organic shale, the results from this experimental study quantitatively differentiating the contribution of OM and clay to the total SSA and pore volume of rock will be helpful to model the adsorption behavior for gas-shale resource assessments and production planning.

6. Conclusions

The pore structure data from this study before and after organic matter removal in samples from different thermal maturity levels reveals important information about pore-structure and textural distribution of organic matter and formation of porosity in OM and its dependence on thermal maturity. Significant conclusions of this study are as follows:

(1) The clay hosted micro- and mesoporosity is the fundamental textural control of mudrock nanostructure and different

textural arrangements between OM and clay mineral pores are observed.

(2) The immature mudrocks have a heterogeneous distribution of OM and clay mineral grain aggregates. The pore-structure may be dominated by clay hosted micro- and meso-porosity, which may be completely open or partially filled by presence of OM.

(3) The OM in the immature mudrocks does not have any evidence of open micro- and fine-scale mesoporosity within OM matrix itself.

(4) Removal of organic matter from thermally mature organic-rich mudrocks resulted in a significant reduction of the pore volume network below a diameter of 5 nm. This reduction of pore volume is an indication of pores hosted within organic matter. These data suggest OM porosity develops in a punctuated manner after the formation reaches a thermal threshold, probably coincident with gas generation.

(5) The relative abundance of micro- and fine meso-pores in mature mudrocks is controlled by both, the clay and the organic contents.

(6) High-pressure methane adsorption potential is controlled by OM content. OM hosted porosity is more efficient in adsorbed methane storage than clay-hosted porosity.

Acknowledgements

The authors thank Chevron Energy Technology Company (ETC), the ATLAB project in Polish Academy of Sciences and the OCLASSH consortium in Colorado School of Mines for supporting this work. The authors acknowledge Artur Kuligiewicz (Institute of Geological Sciences, Polish Academy of Sciences) for his help to collect and analyze the Baltic Basin samples, Marcus Mello (Chevron ETC) and Lin Li (Chevron ETC) for the supercritical methane adsorption data and Kitty Milliken (Bureau of Economic Geology, The University of Texas at Austin) for providing the FESEM image of the Eastern European Shale sample. Thanks to two anonymous reviewers for their constructive suggestions.

References

[1] Passey QR, Bohacs KM, Esch WL, Klimentidis R, Sinha S. From oil-prone source rock to gas-producing shale reservoir – geologic and petrophysical characterization of unconventional shale-gas reservoirs. In: CPS/SPE Int. Oil Gas Conf. Exhib., Beijing, China: 2010.SPE 131350.

[2] Milliken KL, Rudnicki M, Awwiller DN, Zhang T. Organic matter-hosted pore system, Marcellus Formation (Devonian), Pennsylvania. Am Assoc Pet Geol Bull 2013;97:177–200.

[3] Chalmers GRL, Bustin RM. The organic matter distribution and methane capacity of the lower cretaceous strata of Northeastern British Columbia, Canada. Int J Coal Geol 2007;70:223–39.

[4] Ross DJK, Marc Bustin R. The importance of shale composition and pore structure upon gas storage potential of shale gas reservoirs. Mar Pet Geol 2009;26:916–27.

[5] Strąpoć D, Mastalerz M, Schimmelmann A, Drobniak A, Hasenmueller NR. Geochemical constraints on the origin and volume of gas in the New Albany Shale (Devonian–Mississippian), eastern Illinois Basin. Am Assoc Pet Geol Bull 2010;94:1713–40.

[6] Lu X-C, Li F-C, Watson AT. Adsorption measurements in Devonian shales. Fuel 1995;74:599–603.

[7] Zhang T, Ellis GS, Ruppel SC, Milliken K, Yang R. Effect of organic-matter type and thermal maturity on methane adsorption in shale-gas systems. Org Geochem 2012;47:120–31.

[8] Gasparik M, Bertier P, Gensterblum Y, Ghanizadeh A, Krooss BM, Littke R. Geological controls on the methane storage capacity in organic-rich shales. Int J Coal Geol 2014;123:34–51.

[9] Vernik L, Liu X. Velocity anisotropy in shales: a petrophysical study. Geophysics 1997;62:521–32.

[10] Prasad M, Mba KC, Mcevoy TE, Batzle ML. Maturity and impedance analysis of organic-rich shales. SPE Reserv Eval Eng 2011;14(05):533–43.

[11] Zargari S, Prasad M, Mba KC, Mattson ED. Organic maturity, elastic properties, and textural characteristics of self resourcing reservoirs. Geophysics 2013;78(4):D223–35.

[12] Schieber J. Common themes in the formation and preservation of intrinsic porosity in shales and mudstones – illustrated with examples across the phanerozoic. In: SPE Unconv. Gas Conf., Pittsburgh, Pennsylvania, USA: Society of Petroleum Engineers. SPE 132370; 2010.

[13] Curtis ME, Cardott BJ, Sondergeld CH, Rai CS. Development of organic porosity in the Woodford Shale with increasing thermal maturity. Int J Coal Geol 2012;103:26–31.

[14] Loucks RG, Reed RM, Ruppel SC, Hammes U. Spectrum of pore types and networks in mudrocks and a descriptive classification for matrix-related mudrock pores. Am Assoc Pet Geol Bull 2012;96:1071–98.

[15] Tisot PR. Properties of green river oil shale determined from nitrogen adsorption and desorption isotherms. J Chem Eng Data 1962;7:405–10.

[16] Schrodt JT, Ocampo A. Variations in the pore structure of oil shales during retorting and combustion. Fuel 1984;63:1523–7.

[17] Mayer LM. Surface area control of organic carbon accumulation in continental shelf sediments. Geochim Cosmochim Acta 1994;58:1271–84.

[18] Mayer LMLM. Extent of coverage of mineral surfaces by organic matter in marine sediments. Geochim Cosmochim Acta 1999;63:207–15.

[19] Mayer LM, Schick LL, Hardy KR, Wagai R, McCarthy J. Organic matter in small mesopores in sediments and soils. Geochim Cosmochim Acta 2004;68:3863–72.

[20] Han X, Jiang X, Yu L, Cui Z. Change of pore structure of oil shale particles during combustion. Part 1. Evolution mechanism. Energy Fuels 2006;20(6):2408–12.

[21] Han X, Jiang X, Yan J, Liu J. Effects of retorting factors on combustion properties of shale char. 2. Pore structure. Energy Fuels 2011;25:97–102.

[22] Bai J, Wang Q, Jiao G. Study on the pore structure of oil shale during low-temperature pyrolysis. Energy Proc 2012;17:1689–96.

[23] Bernard S, Wirth R, Schreiber A, Schulz H-M, Horsfield B, Hors B. Formation of nanoporous pyrobitumen residues during maturation of the Barnett Shale (Fort Worth Basin). Int J Coal Geol 2012;103:3–11.

[24] Modica CJ, Lapierre SG. Estimation of kerogen porosity in source rocks as a function of thermal transformation: Example from the Mowry Shale in the Powder River Basin of Wyoming. Am Assoc Pet Geol Bull 2012;96:87–108.

[25] Bohacs KM, Passey QR, Rudnicki M, Esch WL, Lazar OR, Upstream E. The spectrum of fine-grained reservoirs from 'shale gas' to 'shale oil'/tight liquids: essential attributes, key controls, practical characterization. Int. Pet. Technol. Conf., Beijing, China; 2013. p. 1–16 [IPTC 16676].

[26] Kuila U, Prasad M. Specific surface area and pore-size distribution in clays and shales. Geophys Prospect 2013;61:341–62.

[27] Gasparik M, Ghanizadeh A, Gensterblum Y, Krooss BM. "Multi-temperature" method for high-pressure sorption measurements on moist shales. Rev Sci Instrum 2013;84:085116.

[28] Gasparik M, Ghanizadeh A, Bertier P, Gensterblum Y, Bouw S, Krooss BM. High-pressure methane sorption isotherms of black shales from The Netherlands. Energy Fuels 2012;26:4995–5004.

[29] Ji L, Zhang T, Milliken KL, Qu J, Zhang X. Experimental investigation of main controls to methane adsorption in clay-rich rocks. Appl Geochem 2012;27:2533–45.

[30] Środoń J, Drits VA, McCarty DK, Hsieh JCC, Eberl DD. Quantitative X-ray diffraction analysis of clay-bearing rocks from random preparations. Clays Clay Miner 2001;49:514–28.

[31] Omotoso O, McCarty DK, Hillier S, Kleeberg R. Some successful approaches to quantitative mineral analysis as revealed by the 3rd Reynolds cup contest. Clays Clay Miner 2006;54:748–60.

[32] Środoń J, Clauer N, Huff W, Dudek T, Banas M. K-Ar dating of the Lower Palaeozoic K-bentonites from the Baltic Basin and the Baltic Shield: implications for the role of temperature and time in the illitization of smectite. Clay Miner 2009;44:361–87.

[33] Topór T, Derkowski A, McCarty DK. Porosity and gas shale formations diagenesis. Clay Miner. Soc. 50th Annu. Meet., N Urbana-Campaign, Illinois, USA; 2013.

[34] Poprawa P. Potencjał występowania złóż gazu ziemnego w łupkach dolnego paleozoiku w basenie bałtyckim i lubelsko-podlaskim. Przegląd Geol 2010;58:226–49.

[35] Poprawa P, Kosakowski P, Wróbel M. Burial and thermal history of the Polish part of the Baltic region. Geol Quart 2010;54:131–41.

[36] McCarty DK. Quantitative mineral analysis of clay bearing mixtures: the Reynolds Cup contest. Int Union Crystallogr Newslett 2002;27:12–6.

[37] Mikutta R, Kleber M, Kaiser K, Jahn R. Review: organic matter removal from soils using hydrogen peroxide, sodium hypochlorite and disodium Peroxo. Soil Sci Soc Am J 2005;69:120–35.

[38] Rouquerol J, Llewellyn P, Rouquerol F. Is the BET equation applicable to microporous adsorbents? Stud Surf Sci Catal 2007:49–56.

[39] Kuila U, Prasad M, Derkowski A, McCarty D. Compositional controls on mudrock pore-size distribution: an example from niobrara formation. In: SPE Annu. Tech. Conf. Exhib., San Antonio, Texas, USA: Society of Petroleum Engineers. SPE 160141; 2012.

[40] Rouquerol F, Rouquerol J, Sing K. Adsorption by powders and porous solids: principles, methodology and applications. Elsevier Ltd.; 1999.

[41] Tiwari P, Deo M, Lin CL, Miller JD. Characterization of oil shale pore structure before and after pyrolysis by using X-ray micro CT. Fuel 2013;107:547–54.

[42] Weiler R, Mills A. Surface properties and pore structure of marine sediments. Deep Sea Res Oceanogr Abstr 1965;12:511–29.

[43] Lewan MD. Assessing natural oil expulsion from source rocks by laboratory pyrolysis. In: Magoon LB, Dow WG, editors. Pet. Syst. source to trap AAPG Mem. 60, Tulsa, Oklahoma: The American Association of Petroleum Geologists; 1994.
[44] Schnackenberg WD, Prien CH. Effect of solvent properties in thermal decomposition of oil shale Kerogen. Ind Eng Chem 1953;45:313–22.
[45] Johnson WF, Walton DK, Keller HH, Couch EJ. In situ retorting of oil shale rubble: a model of heat transfer and product formation in oil shale particles. Q Colo Sch Mines; (United States), vol. 70; 1975. p. 3.
[46] Ambrose RJ, Hartman RC, Diaz-campos M, Akkutlu IY, Sondergeld CH. Shale gas-in-place calculations Part I: New pore-scale considerations. SPE J 2012;01:219–29.